Alteration, mass analysis, and magmatic compositions of the Sentinel Bluffs Member, Columbia River flood basalt province

Michael G. Sawlan

U.S. Geological Survey, 345 Middlefield Road, Menlo Park, CA 94025 MS-973

SUPPLEMENTAL FILE 3

1. METHODS

1.1 Sampling Protocols

Samples were collected using a protocol aimed at minimizing inclusion of altered rock and secondary minerals in the material to be analyzed. Alteration rinds and secondary minerals lining open space and fractures were the principal materials avoided in field sampling. An effort to evaluate the influence of ubiquitous, texturally distinct anastomosing seams, termed "hydration seams", was made by sub-sampling in the lab.

1.1.1 Field Sampling

The typical field sampling protocol is illustrated in Figure S2. Several joint-bounded blocks from the denser parts of flows were broken, compared for sample quality, and one was selected for sampling. Such blocks were commonly 20 to 40 cm across (see Figure S2B), but were smaller where more closely spaced fractures limited the size of the largest unfractured block. Samples were trimmed to remove alteration rinds and pockets of secondary minerals.

Trimming to remove rinds and other altered rock was carried out on an anvil consisting of the same lava with a freshly broken surface (Figure S2D). Progressive trimming was performed until chips ~2 to 4 cm across were obtained. The resulting field sample typically comprised 200-500 g of rock chips (Figure S2E). At least one and often several hand-specimens were also collected.

Only minor attention was given to removal of hydration seams during field sampling. In a field setting, the detailed chipping required to remove such seams would be prohibitively difficult and time consuming.

Figure S1. Field sampling protocol. A) Road-cut exposure of the uppermost Sentinel Bluffs Member flow in the Butler Canyon section (flow BL-8). Lighter gray patches in this photo and in (B) are dried spay from paleomagnetic drilling. B) Joint-bounded block extracted from road cut. C) Part of the block shown in (B) split into large fragments. Secondary mineral(s) lining open space appear as white specks on the freshly broken surface of fragment on the left, inside of a thin weathering rind. Their(?) abundance diminishes 3–6 cm inward from the rind. D) Sample preparation site. Fresh surface of slab used as an anvil is to the right of smaller hammer. Discarded rock fragments are between the hammers. E) "Field-cleaned" rock chips for a geochemical sample and hand specimen. Orange tool shown for scale in photos is 8.8 cm long.

Hydration Seams

Hydration seams are characterized by a resinous texture that obscures the original groundmass texture, and are distributed in intersecting, gently curving layers forming phacoidal

shapes. Nearly all freshly broken rock surfaces, internal to weathering rinds, correspond to surfaces of hydration seams (Figure S2A). Planes of weakness along hydration seams may yield relatively smooth fractures or, where broken internally, form finely "bumpy" surfaces. This relief is inferred to result from intersecting anastomosing surfaces resulting in depressions and crests typically <1 mm across. The texture is distinct from that of interseam rock in which crystalline and amorphous parts of the mesostasis define the texture of surfaces where broken. The thickness of planar parts of hydration seams is commonly 5-12 mm, about twice this thickness where two seams intersect, and even thicker at junctions of three seams. The thickness of interseam rock is commonly 2 cm or less. All samples of Sentinel Bluffs Member lavas collected for the present study contain such seams.

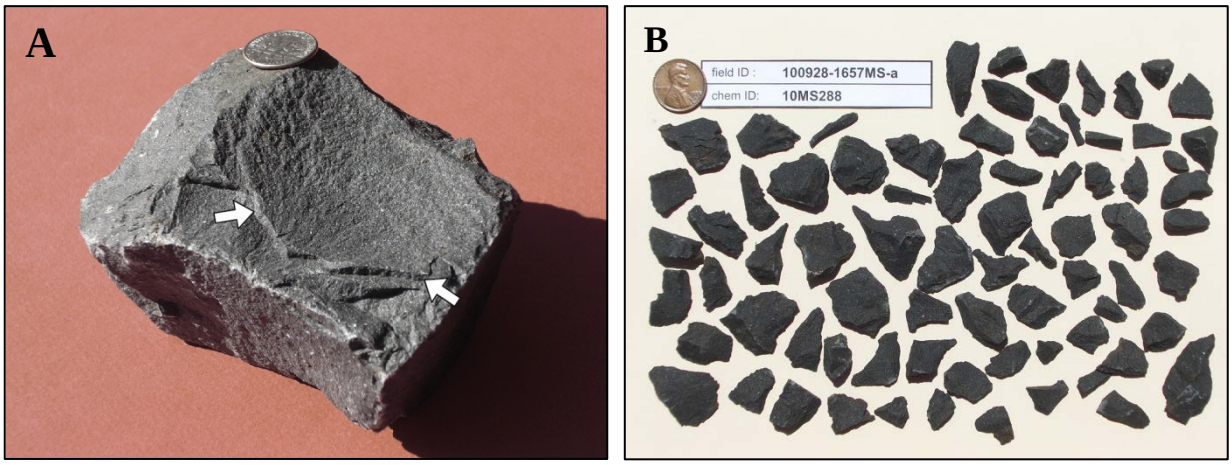

Figure S2. A) Hand-specimen showing surfaces formed by alteration seams. Arrows point to seam forming upper surface. Coin shown for scale is 1.8 cm in diameter. B) Geochemical sample comprising chips of hydration seam. Scale is indicated by coin (1.9 cm diam.).

1.1.2 Laboratory sub-sampling

Detailed trimming of field-cleaned rock chips was performed in the lab to minimize secondary minerals that may have been overlooked during field sampling, and to minimize hydration seams in the material to be analyzed. Field-cleaned chips of geochemical samples were reviewed and described, with particular attention to the presence of secondary minerals. Rock chips were sub-sampled using hammers and an anvil composed of a block of GRB lava, or by sawing.

Field-cleaned chips generally comprise an estimated 60-70% hydration seams. Attempts to remove hydration seams from interseam rock were made only where the thickness of interseam rock was at least 1 cm. Samples of hydration seams were obtained by chipping surfaces of the field-cleaned chips with a hammer. Most or all of a seam thickness typically spalls off the surface of rock chips (<3 cm across) when struck on an edge. Samples of hydration seams consist mainly of thin planar chips; slender chips result from the intersection of two seams, and three-pronged chips result from the intersection of three seams (see Figure S2B). Samples of hydration seams typically contained minimal amounts of interseam rock.

Removal of hydration seams from inter-seam rock was generally less successful due, in most instances, to the minimal thickness (<2 cm) of interseam rock. Chips commonly fracture within hydration seams, leaving thin veneers of seams on the surfaces of mostly interseam rock. This sub-sampling generally reduced the proportion of hydration seams in samples from an estimated 60-70% in field-cleaned chips to some 30-40% in the interseam sample. Most interseam samples therefore consist of concentrates of interseam rock. Samples composed of hammer-trimmed and sawn interseam chips are shown in Figure S3.

Hammer-trimmed rock chips were inspected for hammer marks; those with visible metal smears were discarded. Sawn chips were ground on diamond-embedded stainless steel laps (100 and 180 grit) to remove saw-blade contamination.

Samples provided by R. Evarts were trimmed by sawing hand-specimen-sized or larger blocks of rock to remove material showing visible evidence of alteration. Saw-blade marks were removed by grinding sawn surfaces on a lap with silicon carbide grit. Samples were immersed in an ultrasonic bath to remove grit potentially embedded in void spaces, and allowed to dry at room temperature. The resulting geochemical samples were polyhedral specimens of rock approximately hand-specimen in size, similar in character to the smaller sawn chips shown in Figure S3B.

1.1.3 Paleomagnetic core samples

Samples of paleomagnetic drill core were used for seven geochemical samples at four sites in the Willamette Valley-Coast Range area, at two sites along the lower Columbia River, and at one site in the Bingen section. From each site, as many as four sawn core segments (cylinders 1 inch in length, 0.9 inch in diameter) from the deepest part of each core were selected from the usual

eight cores drilled at each site, and combined into a single geochemical sample (see Figure S3C). As necessary, core cylinders were subsampled by sawing to remove weathering rind or other alteration. Surfaces of the core were ground on diamond laps to remove metal streaks from the drill bit, orienting tool, brass scribe used to orient the core, and any saw marks.

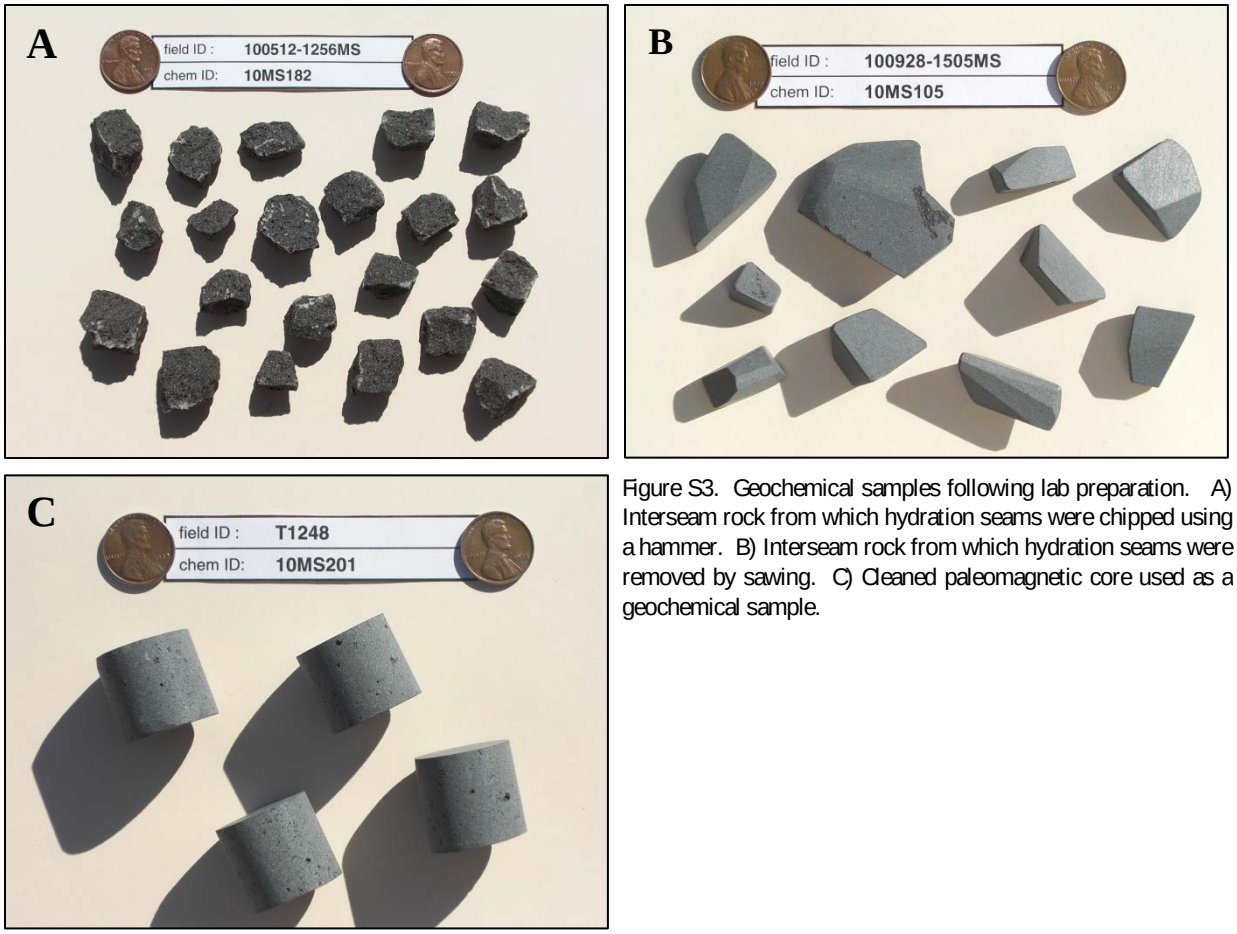

Figure S3. Geochemical samples following lab preparation. A) Interseam rock from which hydration seams were chipped using a hammer. B) Interseam rock from which hydration seams were removed by sawing. C) Cleaned paleomagnetic core used as a geochemical sample.

1.1.4 Sample types

Samples types are characterized in relation to weathering rinds and hydration seams. The analyses in Supplemental File 2 are identified by the sample types given in Table S1.

TABLE S1. SAMPLE TYPES.

Sample Type	Description
interrind	Field-cleaned rock chips from which alteration rinds and macroscopic evidence of alteration were removed. These were subsampled in the lab mainly to exclude any secondary minerals overlooked during field sampling. These samples include hydration seams as well as interseam rock.
interseam	Field-cleaned rock chips from which alteration rinds and macroscopic evidence of alteration were removed, and which were sub-sampled in a lab setting to exclude hydration seams.
hydration seams	Texturally distinct seams comprising anastomosing, curviplanar zones within interseam rock.
interrind-sec. min.	Rock internal to a distinct alteration rind that contains visible secondary minerals (lining open space) in a concentric band along the alteration rind.
alt. rind	Alteration rind, typically darker gray in color than the interrind rock; commonly contains small amounts of clay minerals, iron hydroxide or oxyhydroxide, and likely other secondary minerals, lining or filling open space.
str. weathered	Rock altered under oxic conditions and composed largely if not entirely of secondary minerals (e.g. clay, Fe hydroxide or oxyhydroxide). The one sample of this type analyzed in this study was cut by veins of clay and Fe hydroxide or oxyhydroxide, which were removed from the material submitted for analysis.

1.2 Preparation of Rock Powders

Typically, 90-100 g of rock chips were selected for each geochemical sample. Prior to crushing, samples were weighed and photographed (see Figures S2B and S3). Crushing and pulverization ("grinding") procedures are described below.

1.2.1 Crushing

Rock chips were crushed at the GeoAnalytical Lab using a jaw crusher fitted with heat-tempered, stainless steel plates. This yielded rock fragments that passed an opening having a width of ~4 mm.

For samples prepared by the author, the entire crushed sample, including rock powder generated in the crushing process, was included in the material to be pulverized and analyzed. This differs from the method of hand-picking chips from crushed rock as described in Johnson et al. (1999), and from a practice, apparently more recently employed in the GeoAnalytical Lab, of sieving crushed material to exclude rock powder and smaller rock fragments less than ~1-2 mm across. Such hand-picking or sieving was avoided as it provides an opportunity to fractionate samples by exclusion of softer, more easily crushed parts of samples, such as glassy mesostasis. Also, hydration seams tend to be harder than interseam rock, and upon crushing the seams

typically form broad, thin chips, so that sieving the crushed rock tends to concentrate hydration seams. The crushed samples were split with half to be pulverized and the remainder archived. Typically, 45-50 g of crushed rock was pulverized.

For samples prepared by GeoAnalytical Lab staff, it is assumed that crushed rock chips were sieved or hand picked for the geochemical sample to be pulverized. The method applied to each specific sample was not recorded by the sample preparation staff.

1.2.2 Pulverization

For samples processed in the GeoAnalytical Lab between 2007 and the present, crushed samples were pulverized in a ROCKLABS® Tungsten Carbide 200[1] media. Those samples processed prior to 2007 (6 samples in this study) were pulverized in a SPEX® tungsten carbide media. The SPEX® media contributes minor amounts of Nb contamination (Johnson et al, 1999), whereas the ROCKLABS® media contributes no appreciable contamination of Nb (or Ta) as determined by pulverization and analysis of quartz in this media (R. Conrey, pers. comm., 2011). Ni contamination on the order of approximately 5-10 ppm was observed for the ROCKLABS® media, however, and a correction for this contamination was applied during analysis (R. Conrey, written comm., 2013).

Glass beads of standards used in calibrations were also pulverized in tungsten carbide grinding media following an initial fusion. Calibrations through 2009 used standards ground in a SPEX® tungsten carbide media, and subsequent calibrations used standards ground in the ROCKLABS® media (R. Conrey, pers. comm., 2013). As a result, during 2006-2009 the grinding media differed between standards and analyzed samples. Samples prepared and analyzed during this period have artificially low Ni (5-10 ppm) because a correction for the Ni contamination was applied to samples lacking Ni contamination. Such samples also tend to have slightly lower Nb (average 1.4 ppm) due to analysis of samples ground in media that had no appreciable Nb contamination using calibrations based on standards prepared in media that contributed Nb. The differences in Ni and Nb analyses are apparent in a comparison of 38 samples (20 SB samples from this study and 18 samples from other GRB units (Sawlan, unpubl. data)) initially analyzed in 2009 and reanalyzed in 2013 using calibrations from standards prepared using the same grinding media.

[1] Any use of trade, firm, or product names is for descriptive purposes only and does not imply endorsement by the U.S. Government.

Three analyses reported in this study are for samples prepared and analyzed during the 2006-2009 period. These include two samples from the Patrick Grade section (SB Group 3), and one from the western Columbia River Gorge (SB Group 13). Those samples analyzed with mismatched grinding media between samples and standards can be identified from the analysis dates provided in Supplemental File 2.

1.3 Preparation of fused beads for XRF analysis

A double fusion procedure applied in creating the glass beads for XRF analysis follows that described in Johnson et al. (1999). Minor differences in procedures include changes in the mixing of sample rock powder and flux, and in the polishing of glass beads. Rock powder and flux were mixed using a vortex mixer for approximately 30 seconds. This replaces a 10-minute mixing process using a plastic mixing ball. Polishing of the surface of glass beads was done using a series of diamond-embedded stainless steel laps as opposed to polishing using silicon carbide grit.

1.4 XRF Analysis

All analyses were performed at the Peter Hooper GeoAnalytical Lab at Washington State University in Pullman, Washington, using a ThermoARL Advant'XP+ wavelength-dispersive, sequential X-ray fluorescence spectrometer that was put into service in early 2004. Analytical methods are assumed to follow those described in Johnson et al. (1999), except for several elements as discussed below.

For this study, 100 samples were analyzed during the period 2011-2013 and 12 samples were analyzed during the period 2007-2010. Samples from the Bingen, Butler Canyon, Sentinel Gap, and Devils Hole sections were analyzed within a three-week period, and samples from each section were analyzed sequentially. Dates and times of analyses are given with the XRF analyses in Supplemental File 2.

Although all analyses of this study were performed with the current instrument, analyses performed prior to 2004 are discussed in the main report. Improvements in the accuracy of analyses of Cr and Zr since 2004 are noted below.

1.4.1 Accuracy

Changes in the accuracy of XRF analyses performed at the GeoAnalytical Lab are noted here for elements that are particularly relevant to this study (Cr, Zr), and for elements whose abundances are affected by a mismatch between the grinding media used for samples and standards (Ni, Nb) (see Sec. 1.2.2).

The accuracy of Cr analyses at the GeoAnalytical Lab since 2004 is significantly improved over the values reported in Johnson et al. (1999). The pre-2004 calibrations for Cr resulted in artificially high reported Cr abundances, which are readily apparent in materials having relatively low Cr abundances. For example, for the standard BCR-1 (a sample of a Wapshilla Ridge Member flow, GRB) the value reported by Johnson et al. (1999) is 26 ppm, whereas the recommended value of Govindaraju (1994) is 16 ppm and a more recently determined reference value is 13.5 ± 1.3 (Jochum et al., 2016). This discrepancy, attributed to crystallization of the fused bead for the ultramafic rock standard PCC-1 and its influence on Cr calibrations, was resolved upon the transition to a new XRF instrument in 2004 (R. Conrey, pers. comm., 2013).

The accuracy of Zr analyses at the GeoAnalytical Lab has similarly improved since 2007. Low Zr abundances in earlier SB data are evident in the difference between the value for BCR-1 reported by Johnson et al. (1999) (176 ppm) and the recommended value of 190 ppm (Govindaraju, 1994), which is equivalent to the more recent reference value of 190.3 ± 2.2 (Jochum et al., 2016). The low Zr in the older data is attributed to an incorrect method for background determination. This was resolved in 2007 using a matrix-adjusted background curvature (R. Conrey, pers. comm., 2015).

As described above (see Sec. 1.2.2), the accuracy of Ni and Nb analyses differs as a function of the compositions of the grinding media used for samples and standards. For samples analyzed during the period 2007-2010, when different media were used for samples and standards, Ni abundances are anomalously low by some 5-10 ppm as shown by reanalysis of the same samples using standards prepared with the same media. Also, during this same 2007-2010 period, sample Nb abundances tend to be ~1 ppm low compared to reanalysis post-2010. Twelve analyses of this study were analyzed during the 2007-2010 period. These can be identified by the dates of analyses given in Supplemental File 2.

1.4.2 Precision

The analytical precision of XRF analyses at the GeoAnalytical Lab since 2004 has significantly improved over that of analyses performed with the spectrometer used from the 1980s through mid-2004. The improved precision was remarked upon by Reidel and Tolan (2013), who subdivided some Grande Ronde Basalt (GRB) units based on re-analysis of older glass beads using the current instrument.

Precision estimates provided on the GeoAnalytical Lab website currently consist of single values of precision. These are Limits of Determination (LOD) values determined for selected abundances representing approximately the median abundances of materials commonly analyzed by the GeoAnalytical Lab (R. Conrey, pers. comm., 2013). For this study, a method for estimating precision as a function of abundance was developed and is described below.

Precision estimates applicable to the SB lavas analyzed in the present study are presented in Table S2. These include precision estimates for the maximum and minimum values observed in SB analyses of this study, exclusive of a strongly weathered sample (MI^{53}) for which precision estimates are listed separately.

For this study, precision was estimated from analyses of multiple glass beads prepared from samples used as "internal standards" in the GeoAnalytical Lab. This precision estimate therefore includes uncertainties from sample preparation (following pulverization of rock chips to rock powder) and analytical precision.

The seven internal standards, with the number of analyses in parentheses, include, UMAT1 (28), BCR-C (14), MON01 (6), GMP01 (6), CK442 (10), TED (12), and UM01 (12). Analyses of UMAT1, BCR-C, MON01, GMP01, CK442 were performed in May, 2005; CK442 in January, 2006; and TED and UM01 in June, 2014. Two of these samples are of CRBG lavas and are the UMAT1–Umatilla Member, Saddle Mountains Basalt; and BCR-C–Wapshilla Ridge Member, Grande Ronde Basalt. All analyses were performed with the ThermoARL spectrometer identified above, and were provided courtesy of R. Conrey (pers. comm., 2013 and 2014).

The multiple analyses of each internal standard were used to characterize precision at a particular abundance, taken as the mean value of the analyses of each standard. Precision in terms of 2 standard deviations (2*SD*) was calculated and converted to relative percent of the mean abundance (rel. % 2*SD*). Estimated precision over the entire range of abundances was

determined by fitting an exponential function of the form, $y = b \cdot m^x$, to a log-log plot of rel. % 2*SD* versus abundance (wt. % for oxides, ppm for trace elements) (Figure S4). Values of

Table S2. Estimated precision of XRF analyses of Sentinel Bluffs samples

	Max.*	2*SD*	Min.	2*SD*	CT-3a	2*SD*
SiO_2	55.094	0.061	51.972	0.071	34.901	[0.347]
TiO_2	2.127	0.009	1.695	0.008	2.761	0.010
Al_2O_3	14.864	0.036	13.415	0.034	19.340	0.043
FeO†	12.527	0.074	8.744	0.074	15.848	0.074
MnO	0.255	0.001	0.158	0.001	0.043	0.000
MgO	5.164	0.018	3.747	0.016	0.664	0.015
CaO	9.418	0.030	8.009	0.027	0.427	0.006
Na_2O	3.112	0.016	2.677	0.014	0.035	0.012
K_2O	1.517	0.006	0.833	0.004	0.047	0.001
P_2O_5	0.361	0.002	0.269	0.002	0.183	0.002
Ni	22.1	1.3	9.2	1.4	15.5	1.3
Cr	50.7	1.6	16.0	1.2	43.1	1.5
Sc	39.8	1.3	32.8	1.2	48.2	1.4
V	350.1	4.3	289.8	4.0	322.2	4.1
Ba	850.4	8.2	415.1	5.8	614.3	7.0
Rb	37.3	0.8	18.5	0.7	4.7	0.5
Sr	360.6	2.2	297.9	2.0	25.8	0.9
Zr	179.3	1.8	148.9	1.6	228.0	2.1
Y	56.8	0.9	30.8	0.7	88.8	1.1
Nb	13.3	0.6	10.2	0.6	15.6	0.6
Ga	24.0	1.8	18.3	1.7	29.3	2.0
Cu	43.1	2.9	23.6	2.4	38.8	2.8
Zn	148.7	3.3	110.0	2.8	200.1	3.8
Pb	7.8	1.2	3.7	1.1	5.4	1.1
La	26.3	3.3	14.9	2.9	46.1	3.8
Ce	50.8	3.6	36.1	3.4	20.5	3.3
Th	8.2	1.0	2.1	0.8	5.1	0.9
Nd	30.1	2.5	20.2	2.4	58.6	3.0
U	3.7	2.9	n.d.		1.3	1.7

*Maximum (Max.) and minimum (Min.) values derived from Sentinel Bluffs samples analyzed in this study having MI^s>90. The analysis and precision estimate for a strongly altered sample (MI^s~53) with the identifier CT-3a is listed separately. Values are unnormalized abundances as analyzed. Values for oxides are in weight percent; values for trace elements are in parts per million (ppm).

†Estimates of 2*SD* for FeO are the average 2*SD* in wt. % of the internal standards. FeO is total Fe as FeO.

relative percent 2*SD* were multiplied as needed by a factor of 10^1 or 10^2 to avoid negative values of logarithms. The effect of this multiplier (z) is to shift data points uniformly upward by 1 or 2 log units without affecting their relative distribution, and this factor was later taken into account in calculating precision estimates for a particular abundance. The parameters (m, b) for the

exponential fits determined for each element (except FeO) and the range of values over which this fit was determined are given in Table S3.

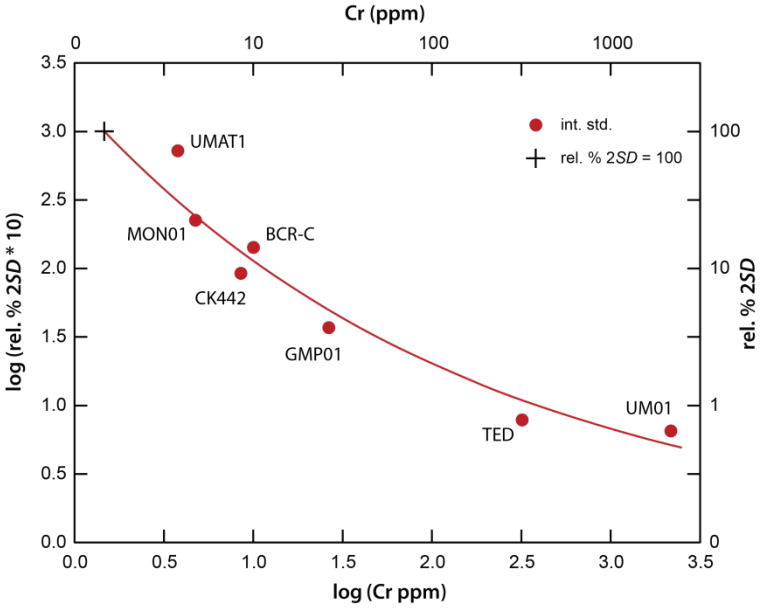

Figure S4. Log-log plot of relative percent 2*SD** 10 versus Cr (in ppm). Each data point (filled red circles) is derived from 6 to 28 analyses of separately prepared fused beads for each sample. The curve is an exponential fit to these data. Data points are labeled by the sample numbers noted in the text. The *LLD* at relative percent 2*SD* equals 100 (plus symbol in figure) corresponds to 1.5 ppm Cr.

Nearly all elements analyzed by XRF at the GeoAnalytical Lab exhibit similar trends in log-log plots of relative percent 2*SD* versus abundance—that is, as abundance decreases the uncertainty, expressed as a percentage of abundance, increases. An exception is observed for the FeO data, which do not exhibit a clear relationship between relative percent 2*SD* and abundance. A precision estimate as a function of abundance therefore could not be determined for the FeO data and, instead, values of 2*SD* (wt. %) from the analyses of internal standards were averaged.

Anomalously high relative percent 2*SD* are apparent among some samples having approximately the same abundance of an element. For instance, high relative percent 2*SD* for some crystalline rocks potentially could be the result of inhomogeneous rock powder rather than resulting only from the uncertainties in fused bead preparation and XRF analysis.

The exponential curve fitted to data for the internal standards enables calculation of precision over a continuous range of elemental abundances. Estimated precision (2*SD*) for abundance *a* is estimated from the following expression

$$2SD = a/z \cdot 10^{-2} \cdot 10^{b \cdot m^{\log^{10}(a)}}, \text{ (S1)}$$

where m and b are the base and constant, respectively, of the exponential curve, and z is a multiplier applied to values of relative percent 2SD, as noted above.

Table S3. Parameters of exponential functions of precision and the compositional ranges of internal standards used in determining the exponential functions

	m	*b*	*z*	Min.*	Max.	comment[†]
SiO_2	0.0384	305.60	100	48.524	71.341	[UM01]
TiO_2	0.5908	0.7295	10	0.005	2.846	
Al_2O_3	0.3881	1.1822	10	0.474	17.230	[MON01]
FeO[‡]	n.d.	n.d.		1.651	12.307	
MnO	0.6872	0.5980	10	0.032	0.212	[UM01]
MgO	0.3687	1.1238	10	0.553	9.354	[UM01]
CaO	0.5542	0.9026	10	0.569	11.516	
Na_2O	0.5180	0.9706	10	0.045	4.022	[MON01]
K_2O	0.5833	0.6197	10	0.001	3.881	
P_2O_5	0.5479	0.5881	10	0.006	0.889	
Ni	0.5783	3.6726	10	5.1	191.8	[UM01]
Cr	0.6353	3.2360	10	3.8	2178	
Sc	0.6351	3.1353	10	3.3	41.8	
V	0.6004	3.9892	10	23.2	409.4	
Ba	0.6253	3.9040	10	5.0	3210	
Rb	0.6483	2.6790	10	0.3	127.4	[CK442]
Sr	0.5504	3.6097	10	4.4	1106	[CK442]
Zr	0.6897	2.3077	10	0.08	488.0	
Y	0.5859	3.0705	10	1.3	49.9	
Nb	0.5844	3.0320	10	0.7	54.9	
Ga	0.7088	3.0245	10	0.7	23.5	
Cu	0.6992	3.2776	10	1.8	64.9	
Zn	0.7049	2.8686	10	41.9	130.5	
Pb	0.6787	3.0785	10	0.6	27.3	
La	0.5444	2.5097	1	0.5	94.4	
Ce	0.4210	3.4079	1	1.2	151.7	
Th	0.6889	2.9098	10	0.4	30.7	
U	0.8492	3.1744	10	0.2	2.9	
Nd	0.6688	3.4928	10	0.9	49.8	

*Minimum (Min.) and maximum (Max.) values indicate the range of abundances of the internal standards used in determining the exponential fits. Values for oxides are in weight percent; values for trace elements are in parts per million (ppm).

[†]Sample IDs given in brackets under "comment" indicate samples excluded from the analysis.

[‡]A systematic relationship is not observed between relative % 2SD and FeO abundance. Value adopted for the precision of FeO analyses is the average uncertainty, in wt. %, for analyses of the internal standards, or 0.74 wt. %.

An empirical estimate of the lower limit of detection (*LLD*) at 2*SD* is obtained by rearranging *Eq*. S1 to solve for abundance *a*, substituting LLD_a, and setting relative percent 2*SD* equal to 100

$$LLD = 10^{\log^m(\log^{10}(z\cdot 10^2/b)}, \text{ (S2)}$$

where *LLD* is in the units as analyzed. This *LLD* corresponds to the abundance at which the relative percent uncertainty at 2*SD* equals 100 percent. In other words, this *LLD* is the value at which 2*SD* and the analyzed abundance are equal.

2. NOTES ON ANALYTICAL RESULTS PRESENTED IN SUPPLEMENTAL FILE 2

2.1 Analyses

Analyses of samples in this study are presented in the spreadsheet provided as Supplemental File 2. Three forms of analyses are presented in separate "sheets", each named "SB" with a suffix indicating the data type, SB.u—unnormalized abundances as reported, SB.n—normalized abundances, and SB.mn—mass-normalized abundances.

For normalized abundances, both major and trace elements are normalized to totals calculated as the sum of major element oxides and trace elements as oxides. Values under the headings Total.M-ox, Total_Tr-ox, and Total_M+Tr-ox correspond to the sum of major element oxides, the sum of trace elements as oxides, and the sum of the major and trace element oxide totals, respectively. The normalization of trace elements is applied to the reported values in ppm.

Analyzed abundances are given as simple numeric values. The normalized and mass-normalized abundances are given as calculated values; the formulas show the relationships between normalized abundances, sample mass index, mass-normalized abundances, and MI^{100}. The sheet named "MI100" contains the slope and intercepts of the MI^{100} lines used in calculating sample mass index (MI^{s},), which, in turn, is used to calculate mass-normalized abundances.

2.2 Supporting Documentation Provided with Analyses

Explanations of supporting documentation presented with the analyses in Supplemental File 2 are given in Table S4. Entries under "Field Name" correspond to column headings in the spreadsheet. A complete set of these data is given in the sheet named "SB.u" containing the unnormalized data; a subset (sample IDs, SB_sec_flow, SB Series and Group, MIs) of these fields is included in the sheets "SB.n" and "SB.mn".

TABLE S4. DESCRIPTION OF SUPPORTING DOCUMENTATION ACCOMPANYING GEOCHEMICAL ANALYSES

Field Name	Description
Chem_ID_field	Sample number assigned to samples when collected. For samples collected by the author, R. Evarts, and R. Wells, the first two digits of sample numbers refer to the year sampled. For samples collected by the author and R. Wells, the first six digits refer to the entire date sampled (in the format yymmdd), followed by a dash and four digits indicating the time of day (in the format hhmm). For samples collected by J. Hagstrum, the sampling year is indicated by the first digit following a prefix consisting of one or two letters; the last three digits refer to individually drilled cores numbered in sequence. Sample numbers that are identical except for the presence or absence of a single letter suffix are subsamples from a single joint-bounded block or adjacent joint-bounded blocks where the joints were closely spaced. An exception to this suffix convention applies to four samples collected nearby in a quarry in the Chapman-Trenholm area (samples a–d from the location collectively identified as 070915-1604-MS).
Chem_ID_lab	Alternate sample numbers assigned to geochemical samples for use by the GeoAnalytical Lab.
Section_ID	The stratigraphic section or general location where sampled. Sections in which two or more SB flows were sampled in stratigraphic succession include Armstrong Canyon, Bingen, Butler Canyon, Devils Hole, Patrick Grade, Sentinel Gap, and Wallace Canyon. Other names refer to general locations or sections in which sampling of SB flows is incomplete: Abernathy Creek, Chapman-Trenholm, Saint Helens, La Center, Western Gorge, Willamette Valley, and Winter Water Creek. Sample locations are given in geographic coordinates (see below). General location references are as follows: Chapman-Trenholm—samples from within two adjoining 7.5-minute quadrangles (Chapman, Trenholm) located west of the cities of Saint Helens and Scappoose, Oregon. Saint Helens—samples from the Saint Helens 7.5-minute quadrangle, Oregon. La Center–samples from the La Center 7.5-minute quadrangle, Washington. The two samples from this area are located in Washington, across the Columbia River from Saint Helens, OR. Western Gorge—one sample from along the west side of Latourell Falls. Willamette Valley—three samples from the Dundee Hills, and several samples from quarries. Winter Water Creek—sample of the lowest SB flow, overlying a flow representing the “type locality” of the Winter Water Member, Grande Ronde Basalt. The SB sample analyzed is the lowest of 3 or 4 SB flows in this section.
SB_Sec_Flow	Entries consist of a two-letter section abbreviation for location followed by a number. For sections in which two or more flows were sampled in succession (see Section_ID, above), the number refers to the number of the SB flow, as defined by contacts, in stratigraphic order (e.g. BG-01 refers to the lowest SB flow in the Bingen section). Although only one SB flow was sampled in the Winter Water Creek section (WW-1), this is the lowest SB flow in this section. Three or four SB flows overlie the flow identified as WW-1, but were not analyzed for this study. For samples from other locations (Western Gorge, Saint Helens, La Center, Willamette Valley, and Abernathy Creek), the number following the location abbreviation was assigned arbitrary.
SB_Series	SB chemical series, numbered from 1 to 5. Numeric values are substituted for the roman numerals used to refer to SB series in the main report.

Field Name	Description
SB_Group	SB chemical group, numbered from 1 to 16.
Sample_type	Identifies samples as interrind, interseam, hydration seams, or inner rind-sec. min. These sample types are described in Table S1 (above).
Site_context	Type of exposure of sampled sites. All samples are from surface exposures consisting of outcrops or artificial exposures of road cuts or quarries.
Sampled_by	Entries identify the scientist who collected the sample in the field. Samplers are identified by surname only. Where two names are separated by slash (e.g. Hagstrum/Sawlan), the second name refers to the person (the author in all instances) who selected from among paleomagnetic core or rocks chips for geochemical samples, and performed additional sample preparation.
Long_NAD83	Longitude in the NAD83 datum. These are negative values indicating longitude west of the Prime Meridian. Methods used in determining sample locations are described below (see Sec. 2.2.1).
Lat_NAD83	Latitude in the NAD83 datum. See note above for Long_NAD83 field.
Chem_prep_type	The method(s) used to exclude altered rock and(or) hydration seams from geochemical samples (see Sampling Protocols, Sec. 1.1). Most samples were chipped using a hammer or sawn with a rock saw. Six samples of paleomagnetic core are indicated as “drilled/sawn – pmag core”.
XRF_Prep_by	The person(s) who performed the sample preparation in creating fused beads for XRF analysis (crushing, grinding, weighing, mixing of rock powder and flux, and fusions) at the GeoAnalytical Lab. Most samples were prepared by the author, others were prepared by GeoAnalytical Lab staff.
XRF_date_time	Date and time of completion of XRF analysis.
MI^s	Sample mass index. Derivation of this value is explained in the main report (see Sec. 3.2), and its calculation is demonstrated in the spreadsheet provided as Supplemental File 3. An explanation of this spreadsheet is provided below (see Sec. 3).

2.2.1 Determination of Geographic Coordinates of Sample Locations

Geographic coordinates of sample locations were determined mainly using GPS measurements. For the continuously sampled sections, locations in the field typically were also mapped on base maps consisting of 7.5-minute topographic maps overlain on NAIP imagery at large scale. In some instances, for example at the base of tall roadcuts and cliffs where GPS reception was poor, GPS measurements were taken at an offset from the outcrop. Using GIS software, GPS locations were compared to NAIP (National Agriculture Imagery Program) imagery and adjusted as necessary. The geographic coordinates given in Supplemental File 2 are from GIS databases.

The accuracy of locations determined with GPS measurements is estimated to be within 6 m or better. Locations of samples from the Butler Canyon section were measured using a high-precision GPS receiver (Trimble GeoXH®) with an external antenna, and with data post-

processing. The accuracy of these measurements is within 1 m, as indicated by measurements repeated at the same location over several days.

Locations of samples collected by R. Wells were determined initially by GPS and later revised in GIS using a LiDAR base. Samples collected by R. Evarts were located by inspection of topographic maps (scale 1:24,000), and are estimated to be accurate within 24 m. Samples from the Chapman and Trenholm quadrangles were located in the field on topographic maps (7.5-minute quads) superposed on NAIP imagery, which were later georeferenced using GIS. Samples collected by J. Hagstrum are from paleomagnetic sites consisting of eight cores typically distributed over a distance of 15-30 m along an exposure. These sites were located with a GPS measurement typically taken within 20 m of one end of the core array.

3. GUIDE TO USING THE MI^{100} CALCULATION SPREADSHEET

The following notes explain the use and function of the spreadsheet provided as Supplemental File 4, which is used to determine MI^{100} "baselines".

3.1 Introduction

The main objectives of the method of iterative calculation of MI^{100} "baselines" are to derive a data-based determination of this line while minimizing the subjectivity in defining it. In the calculation method applied here, this line is determined by iterative regressions of data for two immobile elements within an interval of values of sample mass index (MI^s), or "*MI* window". Two parameters are set by the user and include an initial baseline or "starter" line estimated visually, and the *MI* window.

The determination of a MI^{100} baseline is simplified by the use of an appropriate sampling protocol that minimizes introduced secondary minerals in samples and yields a large number of unaltered or minimally altered samples (see Fig. 5A, main report). The effect of secondary mineral addition is to dilute the abundances of immobile elements, which translates into higher MI^s values. This can potentially exceed mass loss from alteration and, as shown in the examination of earlier analyses of SB data (see Fig. 13, main report), can yield *MI* values in excess of 100. Analyses of samples that contain abundant secondary minerals filling open space (e.g. vesicles, crystal-bounded voids) obviously should be excluded from consideration in MI^{100} determinations.

The calculations used to estimate MI^{100} involve three lines, an initial estimate of MI^{100}, a line used to calculate sample mass index (MI^s_calc), and a third line (MI^{100}_regr) used to calculate MI^{100} by regression of the abundances of two immobile elements (e.g. Al_2O_3 and TiO_2) for those MI^s values within the *MI* window.

3.2 Data Entry

Values entered by the user are highlighted in red. Abundances of TiO_2^n and $Al_2O_3^n$ (or other pair of immobile elements) are entered in columns C and D, respectively. These are abundances normalized to 100 percent volatile-free, as indicated by the superscript *n*. Columns A and B are for sample and unit identifiers, respectively.

Other user-entered values are the coordinates used to define the slope and intercept of an initial estimate of the MI^{100} baseline (cells B4:C5), the *MI* window (cell E3), and the cell under the heading "calculation" (cell G3).

All other cells contain calculated values. Cells shown in blue font are the slope and intercept of MI^{100} for three lines at intermediate(?) stages of the iterative calculations.

3.3 Graph

A plot of Al_2O_3 versus TiO_2, located in the spreadsheet below the last row containing sample data and associated calculated values, shows the sample data points, lines for the MI^{100} regression and upper and lower limits of the *MI* window, and lines having slopes corresponding to the maximum and maximum Al_2O_3/TiO_2 ratio of samples in the dataset. Coordinates for these lines are to the right of the graph. With the number 0 entered in the calculation control cell (G3), the graph shows the visually estimated line and MI window limits. With a 1 (or any non-zero value) entered in cell G3, the lines for MI^{100} and the *MI* window limits are updated as the iterative calculations proceed.

3.4 *MI* Window

The value chosen for the *MI* window depends on the number of samples and their distribution in a bivariate plot of two immobile elements. For the samples in this study, the value for *MI* windows was 0.5 (± 0.25). In general, the value assigned to the *MI* window is dependent on sample population: smaller *MI* windows are appropriate for large datasets and larger *MI* windows are appropriate for smaller datasets. Following an MI^{100} calculation, the value of the *MI*

window is evaluated to assess whether the resulting line is representative of the lower margin of sample Al_2O_3 and TiO_2 abundances. A relatively large *MI* window potentially can include mass-depleted samples in the regression and can result in unaltered samples having artificially high sample mass indexes.

3.5 Initial MI^{100} Estimate

The initial estimate of MI^{100} (MI^{100}_est) is a visually positioned line along the base of the population of samples in a plot of Al_2O_3 versus TiO_2. The distribution of data points with respect to the associated *MI* window is therefore asymmetric. That is, most or all data points are within the low-*MI* half-window (to higher Al_2O_3 and TiO_2) relative to MI^{100}. This line is used only once in the calculations to initialize the slope and intercept values of the other two lines. This line is defined using a pair of coordinates under the heading "coords. for MI^{100}_est" (cells B4-C5). With the number 0 entered in cell G3 (under "calculation"), the graph in the lower part of the spreadsheet is automatically updated and shows the position of the line relative to the sample data.

3.6 Initializing Calculations

After entering TiO_2 and Al_2O_3 data, coordinates for the MI^{100} initial estimate, and a value for the *MI* window, enter the number 0 in the outlined cell under the heading "Calculation" (cell G3). This initializes the values of MI^s_calc and MI^{100}_regr for a new calculation. The slope and intercept of the visually fit initial MI^{100} estimate line are transferred to the slope and intercept of the MI^s_calc and MI^{100}_regr lines. All three lines are therefore identical at the start of calculations. The samples to be included in the regressions of MI^{100} are then determined by iterative calculations.

3.7 Iterative Calculations

The *s*preadsheet contains circular references between the line definitions (slope and intercept) of MI^s_calc and MI^{100}_regr. For calculations to proceed, iterative calculations must be enabled in Excel. Under the File menu, select Options, then Formulas, and check the box "Enable iterative calculation". The default setting in Excel for the maximum number of iterations (100) is usually sufficient. In the calculations performed with data of this study, the slope and intercept for the MI^{100}_regr and MI^s_calc lines reach equality in less than 10 iterations.

Following the first regression calculation, the slope and intercept values of the MI^{100}_regr line are assigned to the MI^{s}_calc line, and a new calculation of the MI^{100}_regr line is performed for a different population of samples included within the *MI* window. These sequential calculations of MI^{s}_calc and MI^{100}_regr continue until the lines MI^{100}_regr and MI^{s}_calc are equal or until the maximum number of iterations (set in File > Options > Formulas) is reached.

3.8 Automatic or Manual Calculation

Calculations can be performed in automatic or manual calculation mode. In Excel, this option is set on the Formulas toolbar, under the Calculation options. In either automatic or manual mode, the "calculation" control value (cell G3) must first be set to 0 to initialize the calculation. To start a calculation, enter 1 (or any other integer) in the "calculation" control value.

3.8.1 Automatic Calculation

When "automatic calculation" is selected, the results appear immediately in the tables and in the graph of Al_2O_3 versus TiO_2, which displays sample data points, the updated MI^{100} line, *MI* window limits, and the maximum and minimum Al_2O_3/TiO_2 ratios for samples in the dataset.

3.8.2 Manual Calculation

When first using the spreadsheet, observing calculations step-by-step is instructive in understanding how the calculations proceed. "Manual calculation" in Excel is selected under File > Options > Formulas. With "Manual calculation" selected, set the "Maximum Iterations" to 1. To step through calculations, select "Calculate Now" by repeatedly pressing the F9 key or, on the Formulas toolbar, clicking the "Calculate Now" button.

A single iteration of MI^{100} calculations is completed for each two worksheet recalculations made (click on "Calculate Now" twice). In the first recalculation, the MI^{100}_regr slope and intercept values are determined; in the second recalculation, the newly calculated MI^{100}_regr slope and intercept values are transferred to MI^{s}_calc. This 2-step process comprises a single iterative calculation.

With each step in manual recalculation, the differences in slope and intercept used in calculating MI^{s} and MI^{100}_regr from the prior step are displayed. Values of Al_2O_3 and TiO_2 along the MI^{100} line, or "parent" Al_2O_3 and TiO_2 values, are recalculated for samples from the

updated MI^{100} line, sample MI^s are recalculated, samples with MI^s within the *MI* window are identified, and Al_2O_3 and TiO_2 values for samples within the *MI* window are copied to columns J and K. The graph of Al_2O_3 versus TiO_2 displays the sample data points, updated MI^{100} line, *MI* window limits, and lines having slopes corresponding to the maximum and maximum Al_2O_3/TiO_2 ratio of samples.

3.9 Description of Cell Contents

Table S5 explains the headings and values in blocks of cells outlined with heavy line borders at the top of spreadsheet, and Table S6 explains the cell contents for the fields identified in row 11 of the spreadsheet.

TABLE S5. DESCRIPTION OF THE CONTENTS OF OUTLINED CELLS

Heading	Content
Coords_MI^{100}_est.	Pairs of TiO_2 and Al_2O_3 values (in cells B4:C5) used to calculate the slope and intercept of the MI^{100}_est. line (cells B7:B9) from a visually estimated line used to initiate calculations.
MI window	User-defined value in *MI* units that are equivalent to weight percent sample mass. This window defines an interval of ±0.5**MI* window relative to MI^{100}.
Calculation	This value initializes calculations when set to 0, and starts calculations when set to 1 (or other non-zero value). Setting this value to 0 sets the line definitions (slope and intercept) of MI^s_*calc* and MI^{100}_regr to be equal to those of the values of MI^{100}_est.
MI^s_*calc*	MI^s values calculated from an interim MI^{100} line and, eventually, a final line. The MI^{100} line is used to calculate TiO_2 and Al_2O_3 values at points along the MI^{100} line that relate to sample abundances in the columns with the headings TiO_2_MI^{100} and Al_2O_3_ MI^{100}. These calculated TiO_2_MI^{100} and Al_2O_3_ MI^{100} values correspond to the intersection of a line having a slope equal to the sample Al_2O_3/TiO_2 ratio with the MI^{100} line.
MI^{100}_regr	Values are the slope and intercept of the MI^{100} line from regression of TiO_2 and Al_2O_3 data for those samples having a MI^s value within the interval 100 ± the half-*MI* window.
Diff MI^{100}_regr_& and MI^s_calc	The differences in slope and intercept between the MI^{100}_regr and MI^s_calc lines.
Summary Table	Reports the number of samples used in the regression, the maximum and minimum MI^s for samples in the regression, the number of samples in the regression having MI^s >100 and <100, the number of samples excluded from the regression having *MI* values greater than the *MI* window, and the maximum calculated MI^s.

TABLE S6. DESCRIPTION OF CELL CONTENTS UNDER THE HEADINGS IN ROW 11 OF SPREADSHEET

Heading	Content
Sample ID	Entry for sample number.
Unit ID	Entry for a unit identifier.
TiO_2^n	Sample TiO_2^n (from analysis normalized to 100 percent, volatile-free).
$Al_2O_3^n$	Sample $Al_2O_3^n$ (from analysis normalized to 100 percent, volatile-free).
TiO_2_MI^{100}	TiO_2 abundance calculated from MI^{100}_est.
Al_2O_3_MI^{100}	Al_2O_3 abundance calculated from MI^{100}_est.
MI^s	Calculated sample mass index.
in *MI* window	Comparison of MI^s to an *MI* interval equal to 100 +/- the *MI* window. Value is "OK" if MI^s is within the MI window (>=MI^{min} and <= MI^{max}). Value is "high MI" if $MI^s > MI^{max}$. Value is null if $MI^s < MI^{min}$.
TiO_2 in *MI* win.	TiO_2 values for those samples having MI^s within the *MI* window.
Al_2O_3 in *MI* win.	Al_2O_3 values for those samples having MI^s within the *MI* window.
MI^s_win	MI^s_values for samples within the *MI* window
Al_2O_3/TiO_2	Al_2O_3/TiO_2 ratios for all samples

4. REFERENCES CITED

Govindaraju, K., 1994, Compilation of working values and sample description for 383 geostandards: Geostandards Newsletter, vol. 18, Special Issue, p. 1-158.

Jochum, K. P., Weis, U., Schwager, B., Stoll, B., Wilson, S.A., Haug, G.H., Andreae, M.O., and Enzweiler, J., 2016, Reference values following ISO guidelines for frequently requested rock reference materials: Geostandards and Geoanalytical Research, v. 40, p. 333–350, doi: 10.1111/j.1751-908X.2015.00392.x.

Johnson, D.M., Hooper, P.R., and Conrey, R.M., 1999, XRF analysis of rocks and minerals for major and trace elements on a single low dilution Li-tetraborate fused bead: Advances in X-ray Analysis, v. 41, p. 843–867.

Reidel, S.P., and Tolan, T.L., 2013, The Grande Ronde Basalt, Columbia River Basalt Group, *in* Reidel, S.P., Camp, V.E., Ross, M.E., Wolff, J.A., Martin, B.S., Tolan, T.L., and Wells, R.E., eds., The Columbia River Flood Basalt Province: Geological Society of America Special Paper 497, p. 117–153, doi:10.1130/2013.2497(05).